A CALCULATION METHOD AND DATA FOR THE DYNAMIC COEFFICIENTS OF OIL-LUBRICATED JOURNAL BEARINGS

J. W. Lund and K. K. Thomsen

Department of Machine Elements
The Technical University of Denmark
Lyngby, Denmark

ABSTRACT

A numerical method for calculating the stiffness and damping coefficients of oil-lubricated bearings is presented. It is a finite difference solution of Reynolds' equation, obtaining not only the steady-state pressure distribution, but also the dynamic pressures produced by a small amplitude whirl of the journal center (a first order perturbation solution). Film rupture is taken into account with the boundary to the ruptured film zone determined by an iterative procedure.An integration of the pressure yields the load carrying capacity, the four stiffness coefficients, and the four damping coefficients. Data are given in tabular form for the two-axial groove bearing, the elliptical bearing, the three-lobe bearing, and the offset cylindrical bearing.

NOMENCLATURE

B_{xx}, B_{xy}, B_{yx}, B_{yy} = damping coefficients, N·sec/m

C = radial clearance, m

c_v = specific heat of lubricant per unit volume, N·m/m^3°C

D = journal diameter, m

e = journal center eccentricity, m

F_x, F_y = bearing reaction force components, N

h = film thickness, m

K_{xx}, K_{xy}, K_{yx}, K_{yy} = stiffness coefficients, N/m

L = bearing length, m

N = rotational speed, rps

P = friction power loss, N·m/sec

p = film pressure, N/m^2

Q = side flow (no contribution from grooves), m^3/sec

R = journal radius, m

S = Sommerfeld number

T = temperature, ^oC

t = time, sec

W = static load, N

x,y = journal center coordinates, m

z = axial coordinate for bearing film, m

δ = preload, d/C (see Fig.2)

ε = eccentricity ratio, e/C (see Fig.2)

θ = angular coordinate for bearing film

κ = effective bearing stiffness, N/m

μ = lubricant viscosity, $N\cdot sec/m^2$

ν = instability whirl frequency, rad/sec

ϕ = attitude angle (see Fig.2)

ψ_p = position angle for center of curvature of segment no. p (see Fig.2)

$\omega = 2\pi N$, angular speed of rotation, rad/sec

Subscripts

0 = static equilibrium position

p = bearing segment number

INTRODUCTION

Design calculations of the dynamic behaviour of rotors rely on an accurate representation of the dynamic characteristics of the bearings. The bearings are often the major source of damping, and their stiffness properties affect the critical speeds and the stability of the rotor. Hence, it is important to have efficient methods available to calculate the bearing coefficients, and it is the purpose of this paper to describe one such method. In addition, dimensionless data are given for four representative bearing types.

In order to illustrate the application of the method to rotor dynamics problems and, also, its extension to other bearing types (pivoted shoe bearings, gas bearings, etc.), the reference list cites publications by the authors which are related to the present paper.

As the list would otherwise become too long, no further references are give, although numerous important contributions are to be found in the literature.

The Dynamic Bearing Coefficients.

The load carrying capacity of fluid film bearings derives from the hydrodynamic pressures produced in the lubricant film by the shearing action of the rotating journal. At any given speed where also the lubricant viscosity is known, the film reaction force, F, is a function of the journal center position relative to the bearing center and, in addition, it depends on the instantaneous journal center velocity (the squeeze effect).

In referring to Fig. 2 a cartesian coordinate system is introduced with the x-axis pointing vertically downwards (in the static load direction) and the y-axis horizontal. Thus, at a given angular speed, ω, the reaction force is a function of x, y, $\dot{x}$ and $\dot{y}$ ("dot" indicates differentiation with respect to time). With components F_x and F_y in the negative x and y-directions the force may be written as:

$$F_x = F_x(x,y,\dot{x},\dot{y};\omega) \qquad F_y = F_y(x,y,\dot{x},\dot{y};\omega) \tag{1}$$

The static equilibrium position, where $\dot{x}=\dot{y}=0$, has the coordinates (x_o,y_o) such that, when W is the static load:

$$F_{xo}=F_x(x_o,y_o,0,0;\omega)=W \qquad F_{yo}=F_y(x_o,y_o,0,0;\omega)=0 \tag{2}$$

For a small amplitude motion with amplitudes Δx and Δy around the equilibrium position a first order Taylor expansion may be employed to express the dynamic part of the reaction force as:

$$\begin{aligned} \Delta F_x &= F_x - F_{xo} = K_{xx}\Delta x + K_{xy}\Delta y + B_{xx}\Delta\dot{x} + B_{xy}\Delta\dot{y} \\ \Delta F_y &= F_y - F_{yo} = K_{yx}\Delta x + K_{yy}\Delta y + B_{yx}\Delta\dot{x} + B_{yy}\Delta\dot{y} \end{aligned} \tag{3}$$

where the K's are stiffness coefficients and the B's are damping coefficients. They are the gradients of the reaction force, evaluated in the equilibrium position:

$$K_{xx} = \left(\frac{\partial F_x}{\partial x}\right)_o \qquad K_{xy} = \left(\frac{\partial F_x}{\partial y}\right)_o$$

$$B_{xx} = \left(\frac{\partial F_x}{\partial \dot{x}}\right)_o \qquad B_{xy} = \left(\frac{\partial F_x}{\partial \dot{y}}\right)_o \tag{4}$$

and similarly for the remaining coefficients. They may be calculated from a perturbation solution as shown in the Appendix.

For the coefficient indicies, the first index gives the force direction and the second index the displacement direction. In the literature, a different coordinate system is frequently used where the x-axis gives the radial direction (the line connecting the centers of the bearing and the journal) while the y-axis is the tangential direction. Because the journal equilibrium position shifts with operating conditions, this coordinate system changes orientation with speed which is inconvenient in rotor dynamics calculations. The coefficients, however, are readily transformed into the fixed coordinate system which is also necessary when a comparison is performed.

Although equation(3) theoretically is only valid for infinitesimal amplitudes it is found in practice to hold for amplitudes as large as up to one half of the radial clearance, thus covering the range of interest in most applications. The error introduced by replacing the highly non-linear reaction force by linear coefficients is partly offset by the softening-hardening stiffness characteristic of the force, and partly by a shift towards the bearing center of the mean position around which the motion takes place. Thus, as the journal whirl orbit grows larger its center no longer coincides with the static equilibrium position but moves gradually closer to the bearing center. This is of secondary importance, however, as it is usually the amplitude of the vibration which is of interest, and not its D.C.-level.

It should furthermore be recognized that the solution of the lubrication equation (Reynolds' equation) normally is based on several simplifications, such as the assumption of constant viscosity, and such as some hypothesis for the mechanism of film rupture which may not be adequate under dynamic conditions.When adding that the actual

operating bearing temperature and, hence, the effective viscosity cannot be predicted too accurately, and that manufacturing tolerances may play a significant role, the approximate representation of the bearing by stiffness and damping coefficients is satisfactory for most practical purposes. This seems confirmed by experiments [10,12,13].

The coefficients may be used directly in rotor dynamics calculations for unbalance response, random vibration response, and for determining the damped critical speeds and rotor instability[10,11]. As the coefficients belong to some given equilibrium postion they actually become functions of speed, and for that reason any particular rotor calculation always applies at a specified speed value.

The destabilizing property of the bearing coefficients stems from the lack of symmetry in the stiffness coefficients where K_{xy} and K_{yx} are unequal (the damping coefficients are symmetric ($B_{xy}=B_{yx}$)).

Instability sets in at that speed where the static equilibrium position no longer is dynamically stable and where the journal, therefore, begins to whirl in a small orbit around the equilibrium position. The whirl frequency, ν, usually coincides with the lowest natural frequency of the rotor system (not necessarily the same frequency as the first critical speed), and the ratio between whirl frequency and rotational frequency is typically around ½ or less.

The whirl behaviour past the threshold speed cannot, of course, be analyzed on the basis of the linear coefficients, but experience shows that in most applications the whirl orbit grows very rapidly such that the calculated threshold speed should be considered as the limiting speed for safe operation in practice.

The threshold speed depends not only on the bearings, but also on the rotor, and where the bearings are located. For any given rotor-bearing system it is therefore necessary to determine the threshold speed by a complete system calculation[11]. In order, however, to have some basis for comparing different bearing types a frequently employed method is to assume the rotor to be rigid and symmetric, whereby each of the two bearings may be assigned a journal mass equal to one half of the rotor mass. It then becomes possible to determine a critical journal mass, M_{crit}, as the upper limit for stability:

$$M_{crit} = \frac{\kappa}{\nu^2} \tag{5}$$

where κ is an effective bearing stiffness:

$$\kappa = \frac{K_{xx}B_{yy}+K_{yy}B_{xx}-K_{xy}B_{yx}-K_{yx}B_{xy}}{B_{xx}+B_{yy}} \tag{6}$$

while the instability whirl frequency is found from:

$$(\frac{\nu}{\omega})^2 = \frac{(K_{xx}-\kappa)(K_{yy}-\kappa)-K_{xy}K_{yx}}{\omega B_{xx}\omega B_{yy}-\omega B_{xy}\omega B_{yx}} \tag{7}$$

Because the coefficients are functions of speed, so is the critical mass. Hence, the instability threshold speed is determined by that speed at which the actual journal mass equals the critical mass.

The critical mass may be considered as a measure of a particular bearing type's sensitivity to instability. As an example, of the four types considered below, the critical mass for the two-axial groove bearing is less than 1/3 of the critical mass for the other three bearing types.

On the other hand, when considering the more common case of a flexible rotor, the whirl frequency may be a better indicator than the critical mass because instability sets in when the whirl frequency equals the fundamental natural frequency of the system (exceptions may be found). Hence, while the two-axial groove bearing, the elliptical bearing and the three-lobe bearing tend to have frequency ratios, ν/ω, of approximately 0.4-0.5 over most of the speed range, the ratio for the offset cylindrical bearing is significantly lower such that this bearing type may be expected to be more stable. For any particular application, however, only a complete analysis of the rotor-bearing-system can decide the question, and as an example, there are instances where the actual flexible rotor has a higher threshold speed than the equivalent rigid rotor.

Data Tables

Tables 1 to 4 give dimensionless data for four bearing types, see Fig. 1, at two length-to-diameter ratios, namely L/D=0.5 and 1. With the symbols otherwise defined in the nomenclature, the values in the tables are:

$$S = \frac{\mu NDL}{W}\left(\frac{R}{C}\right)^2 \qquad \text{(Sommerfeld number)} \tag{8}$$

$\varepsilon = e/C$, see Fig.2 (eccentricity ratio relative to bearing center) (9)

ϕ = attitude angle, degrees, see Fig.2 (relative to bearing center)

$$\bar{Q} = Q/\tfrac{1}{2}\pi NDLC \qquad \text{(dimensionsless side flow)} \tag{10}$$

$$\bar{P} = CP/\pi^3\mu N^2 LD^3 \qquad \text{(dimensionless friction power loss)} \tag{11}$$

$$\bar{T} = \Delta T/\frac{\mu\omega}{c_v}\left(\frac{R}{C}\right)^2 \qquad \text{(dimensionless temperature rise, loaded sement)} \tag{12}$$

$$\bar{K}_{xx},\bar{K}_{xy},\bar{K}_{yx},\bar{K}_{yy} = \frac{CK_{xx}}{W},\frac{CK_{xy}}{W},\frac{CK_{yx}}{W},\frac{CK_{yy}}{W} \quad \text{(dimensionless stiffness coefficients)} \tag{13}$$

$$\bar{B}_{xx},\bar{B}_{xy},\bar{B}_{yx},\bar{B}_{yy} = \frac{C\omega B_{xx}}{W},\frac{C\omega B_{xy}}{W},\frac{C\omega B_{yx}}{W},\frac{C\omega B_{yy}}{W} \quad \text{(dimensionless damping coefficients)} \tag{14}$$

The side flow, Q, is the total side flow (both sides) for the bearing, excluding any contribution from the grooves. The friction power loss, P, includes the losses in the ruptured film zone.

The lubricant viscosity, μ, depends on the oil temperature which, in lieu of measurements, can only be established approximately. By assuming that 80 per cent of the friction heat is carried away by the oil, the over-all operating temperature of the bearing is found from:

$$T_{operat} = T_{supply} + 0.8\frac{\mu\omega}{c_v}\left(\frac{R}{C}\right)^2 4\pi\frac{\bar{P}}{\bar{Q}} \tag{15}$$

where T_{supply} is the oil supply temperature. The maximum temperature of the oil occurs in the loaded bearing segment and becomes:

$$T_{max} = T_{operat} + \Delta T = T_{operat} + \frac{\mu\omega}{c_v}\left(\frac{R}{C}\right)^2\bar{T} \tag{16}$$

where $\bar{T}$ is given in the tables.

The temperature, T_{max}, should be used as the one which determines the viscosity, μ, and it is found by an iterative procedure. Be-

ginning with an estimated temperature value the corresponding viscosity value can be obtained from a viscosity-temperature diagram for the lubricant, making it possible to compute the Sommerfeld number, S, and thereafter enter the bearing data table to determine $\bar{Q}$, $\bar{P}$ and $\bar{T}$. With these values, T_{max} can be calculated from equations(15) and (16), and if the result differs from the originally estimated temperature value, the procedure is repeated until convergence has been achieved.

With the established value of the Sommerfeld number the dynamic bearing coefficients can be obtained from the data tables, usually requiring interpolation.

It should be noted that the tables give the eccentricity ratio, ε, and the attitude angle, ϕ, for the static equilibrium position of the journal center relative to the bearing center. For the preloaded bearing types, however, it is the eccentricity ratio, ε_p, and the associated angle, ϕ_p, relative to the center of curvature of the bearing segments which is if interest. Referring to Fig. 2 the relationships are:

$$\begin{aligned} e_p\cos\phi_p &= e\cos\phi - d\cos\psi_p \\ e_p\sin\phi_p &= e\sin\phi - d\sin\psi_p \end{aligned} \qquad (17)$$

where d is the distance from the center of curvature to the bearing center, and ψ_p gives the angular location from the x-axis. The preload, δ, is defined as:

$$\delta = d/C \qquad (18)$$

where C is the radial clearance (the difference between the radius of curvature for the segment, and the journal radius). Hence, equation(17) yields:

$$\varepsilon_p = e_p/C = \sqrt{\varepsilon^2+\delta^2-2\varepsilon\delta\cos(\psi_p-\phi)} \qquad (19)$$

$$\tan\phi_p = \frac{\varepsilon\sin\phi-\delta\sin\psi_p}{\varepsilon\cos\phi-\delta\cos\psi_p} \qquad (20)$$

When the value of ϕ_p falls within the borders of the segment the minimum film thickness is given by:

$$h_{min} = C(1-\varepsilon_p) \tag{21}$$

Usually, h_{min} is located in the loaded segment (the bottom segment) in which case ψ_p is equal to 180 degrees for the elliptical bearing and the three-lobe bearing while ψ_p equals 270 degrees for the offset cylindrical bearing. The preload, δ, is 0.5 for the three bearing types.

REFERENCES

1 Pinkus, O. and Sternlicht, B., "Theory of Hydrodynamic Lubrication", McGraw-Hill Book Company, Inc., 1961

2 Castelli, V. and Pirvics, J., "Equilibrium Characteristics of Axial-Groove Gas-Lubricated Bearings", Journal of Lubrication Technology, Trans. ASME, Series F, Vol. 89, No. 2, April 1967, pp. 177-196.

3 Lund, J.W., "Rotor-Bearing Dynamics Design Technology, Part VII: The Three Lobe Bearing and Floating Ring Bearing", Report No. AFAPL-TR-65-45, Part VII, Wright-Patterson Air Force Base, Ohio, Feb. 1968.

4 Lund, J.W., "Rotor-Bearing Dynamics Design Technology, Part III: Design Handbook for Fluid Film Type Bearings", Report No. AFAPL-TR-65-45, Part III, Wright-Patterson Air Force Base, Ohio, May 1965.

5 Lund, J.W., "Spring and Damping Coefficients for the Tilting Pad Journal Bearing", Trans. ASLE, Vol. 7, 1964, pp. 342-352.

6 Lund, J.W., "Calculation of Stiffness and Damping Properties of Gas Bearings", Journal of Lubrication Technology, Trans. ASME, Series F, Vol. 90, 1968, pp. 793-803.

7 Reinhardt, E. and Lund, J.W., "The Influence of Fluid Inertia on the Dynamic Properties of Journal Bearings", Journal of Lubrication Technology, Trans. ASME, Series F, Vol. 97, No. 2, April 1975, pp. 159-167.

8 Thomsen, K.K. and Lund, J.W., "Consideration of Film Rupture in the Inlet Zone of a Journal Bearing", Proc. 1st Leeds-Lyon Symposium on Tribology: Cavitation and Related Phenomena in Lubrication, edit. D. Downson and C.M. Taylor, The Institution of Mech. Engineers, London, 1975, pp. 163-167.

9 Lund, J.W. and Saibel, E., "Oil Whip Whirl Orbits of a Rotor in Sleeve Bearings", Journal of Engineering for Industry, Trans. ASME, Series B, Vol. 89, No. 4, Nov. 1967, pp. 813-823.

10 Lund, J.W. and Orcutt, F.K., "Calculations and Experiments on the Unbalance Response of a Flexible Rotor", Journal of Engineering for Industry, Trans. ASME, Series B, Vol. 89, No. 4, Nov. 1967, pp. 785-796.

11 Lund, J.W., "Stability and Damped Critical Speeds of a Flexible Rotor in Fluid-Film Bearings", Journal of Engineering for Industry, Trans. ASME, Series B, Vol. 96, No. 2, May 1974, pp. 509-517.

12 Christensen, E., Tonnesen, J. and Lund, J.W., "Dynamic Film

Pressure Measurements in Journal Bearings for Use in Rotor Balancing", Journal of Engineering for Industry, Trans. ASME, Series B, Vol. 98, No.1, Feb. 1976, pp. 92-100.

13 Tonnesen, J. and Lund, J.W., "Some Experiments on Instability of Rotors Supported in Fluid-Film Bearings", Journal of Mechanical Design, Trans. ASME, Paper No. 77-DET-23, Design Engineering Technical Conference, Chicago, Ill., Sept. 26-30, 1977.

APPENDIX

The governing equation for the pressure in the bearing film is Reynolds' equation:

$$\frac{1}{R^2}\frac{\partial}{\partial\theta}\left(\frac{h^3}{12\mu}\frac{\partial p}{\partial\theta}\right) + \frac{\partial}{\partial z}\left(\frac{h^3}{12\mu}\frac{\partial p}{\partial z}\right) = \tfrac{1}{2}\omega\frac{\partial h}{\partial\theta} + \frac{\partial h}{\partial t} \tag{22}$$

where p is the film pressure, μ is the viscosity, ω is the angular speed of rotation, t is time, z is the axial coordinate, and θ is the circumferential coordinate angle. When θ is measured from the vertical load line (the negative x-axis) the film thickness h is given as:

$$h = C + e_p\cos(\theta-\phi_p) \tag{23}$$

where C is the radial clearance and e_p is the displacement of the journal center from the center of curvature of the bearing pad. The attitude angle, ϕ_p, gives the angle from the x-axis to the line connecting the two centers (see Fig. 2).

In static equilibrium the journal center position is defined by the eccentricity e_{op} and the attitude angle ϕ_{op}. Under dynamic conditions the journal center motion is described by the amplitudes Δx and Δy, measured from the static equilibrium position, such that the film thickness becomes:

$$h = h_o + \Delta x\cos\theta + \Delta y\sin\theta \tag{24}$$

where

$$h_o = C + e_{op}\cos(\theta-\phi_{op}) \tag{25}$$

By assuming the amplitudes to be small, a first order expansion of the pressure can be written as:

$$p = p_o + p_x \Delta x + p_y \Delta y + p_{\dot{x}} \Delta \dot{x} + p_{\dot{y}} \Delta \dot{y} \tag{26}$$

where p_o is the film pressure under static equilibrium conditions. "Dot" denotes differentiation with respect to time.

Upon substitution of equations(24) and (26) into equation(22) and retaining first order terms only, five equations are obtained:

$$\left\{\frac{1}{R^2}\frac{\partial}{\partial\theta}\left(\frac{h_o^3}{12\mu}\frac{\partial}{\partial\theta}\right) + \frac{\partial}{\partial z}\left(\frac{h_o^3}{12\mu}\frac{\partial}{\partial z}\right)\right\}\begin{Bmatrix} p_o \\ p_x \\ p_y \\ p_{\dot{x}} \\ p_{\dot{y}} \end{Bmatrix}$$

$$= \begin{Bmatrix} \frac{1}{2}\omega\frac{\partial h_o}{\partial\theta} \\ -\frac{1}{2}\omega\left(\sin\theta + 3\frac{\cos\theta}{h_o}\frac{\partial h_o}{\partial\theta}\right) - \frac{h_o^3}{4\mu}\frac{1}{R^2}\frac{\partial p_o}{\partial\theta}\frac{\partial}{\partial\theta}\left(\frac{\cos\theta}{h_o}\right) \\ \frac{1}{2}\omega\left(\cos\theta - 3\frac{\sin\theta}{h_o}\frac{\partial h_o}{\partial\theta}\right) - \frac{h_o^3}{4\mu}\frac{1}{R^2}\frac{\partial p_o}{\partial\theta}\frac{\partial}{\partial\theta}\left(\frac{\sin\theta}{h_o}\right) \\ \cos\theta \\ \sin\theta \end{Bmatrix} \tag{27}$$

The boundary conditions are that the pressure is zero at the edges of the bearing pad:

$$\underline{z = \pm\frac{L}{2}}$$

$$\underline{\theta = \theta_{1p}} \quad : p = 0 \rightarrow p_o = p_x = p_y = p_{\dot{x}} = p_{\dot{y}} = 0 \tag{28}$$

$$\underline{\theta = \theta_{2p}}$$

where L is the bearing length, θ_{1p} gives the position of the leading edge of the pad, and θ_{2p} gives the trailing edge.

Because of symmetry around the centerplane, only one half of the bearing film needs to be considered which means that the boundary conditions at $z = -\frac{L}{2}$ is replaced by:

$$\underline{z = 0} : \frac{\partial p}{\partial z} = 0 \rightarrow \frac{\partial p_o}{\partial z} = \frac{\partial p_x}{\partial z} = \frac{\partial p_y}{\partial z} = \frac{\partial p_{\dot{x}}}{\partial z} = \frac{\partial p_{\dot{y}}}{\partial z} = 0 \qquad (29)$$

The trailing edge at $\theta=\theta_{2p}$ is either at an axial supply groove or, when the groove is in the diverging part of the film ($\phi_{op}+180^o<\theta_{2p}<\phi_{op}+360^o$), it is the free boundary where film rupture sets in. In this case θ_{2p} becomes a function of z, and the boundary curve is located by the condition that, in addition to the pressure being zero along the curve, the pressure gradient normal to the curve is also zero:

$$\underline{\theta = \theta_{2p}(z)}: p = \frac{\partial p}{\partial n} = 0 \rightarrow p = \frac{\partial p}{\partial \theta} = \frac{\partial p}{\partial z} = 0 \qquad (30)$$

By means of this condition the boundary curve is determined by an iterative procedure when solving for the static pressure, p_o, as discussed later. Under dynamic conditions a point on the curve with coordinates (θ_o,z_o) moves to a new position: $\theta = \theta_o+\Delta\theta, z = z_o+\Delta z$, and requiring the pressure to be zero also on the new boundary a first order expansion yields:

$$p(\theta,z) = 0 = p(\theta_o,z_o)+(\frac{\partial p}{\partial \theta})_o\Delta\theta+(\frac{\partial p}{\partial z})_o\Delta z \qquad (31)$$

By writing equation(26) as: $p=p_o+\Delta p$, substituting it into equation (31) and retaining first order terms only, leads to:

$$p(\theta,z) = 0 = p_o(\theta_o,z_o)+\Delta p(\theta_o,z_o)+(\frac{\partial p_o}{\partial \theta})_o\Delta\theta+(\frac{\partial p_o}{\partial z})_o\Delta z \qquad (32)$$

from which it is seen that: $\Delta p(\theta_o,z_o)=0$ because p_o and its gradients are zero on the original boundary curve. Hence, the boundary conditions at the film rupture boundary are:

$$\underline{\theta = \theta_{2p}(z)}: \quad p_o = \frac{\partial p_o}{\partial \theta} = \frac{\partial p_o}{\partial z} = 0$$

$$p_x = p_y = p_{\dot{x}} = p_{\dot{y}} = 0 \qquad (33)$$

The leading edge at $\theta=\theta_{1p}$ is either at a supply groove or, when the groove is in the diverging part of the film, it is taken to be at maximum film thickness where $\theta_{1p}=\phi_{op}$. This seems to be a reasonable approximation to the actual physical situation as long as an adequate understanding of the problem of film formation is lacking. Indications are that the film forms slightly ahead of the maximum film, but the choice of location proves not to affect the final result by very much.

With the given boundary conditions, the five equations, equation (27), can be solved numerically as discussed below after which the pressures are integrated over the film domain to get the reaction forces from the film.

By summing over all pads making up the bearing, the reaction forces are obtained as:

$$\begin{Bmatrix} F_x \\ F_y \end{Bmatrix} = \begin{Bmatrix} F_{xo}+K_{xx}\Delta x+K_{xy}\Delta y+B_{xx}\Delta\dot{x}+B_{xy}\Delta\dot{y} \\ F_{yo}+K_{yx}\Delta x+K_{yy}\Delta y+B_{yx}\Delta x+B_{yy}\Delta y \end{Bmatrix} = \sum_p -2 \int_0^{\frac{1}{2}L} \int_{\theta_{1p}}^{\theta_{2p}} p \begin{Bmatrix} \cos\theta \\ \sin\theta \end{Bmatrix} Rd\theta dz \qquad (34)$$

As index o gives the static equilibrium position, F_{xo} equals the static load W while F_{yo} must be zero:

$$\begin{Bmatrix} F_{xo} \\ F_{yo} \end{Bmatrix} = \begin{Bmatrix} W \\ 0 \end{Bmatrix} = \sum_p -2 \int_0^{\frac{L}{2}} \int_{\theta_{1p}}^{\theta_{2p}} p_o \begin{Bmatrix} \cos\theta \\ \sin\theta \end{Bmatrix} Rd\theta dz \qquad (35)$$

By substituting for p from equation(26) it is furthermore found that:

$$\begin{Bmatrix} K_{xx} \\ K_{yx} \end{Bmatrix} = \sum_p -2 \int_0^{\frac{L}{2}} \int_{\theta_{1p}}^{\theta_{2p}} p_x \begin{Bmatrix} \cos\theta \\ \sin\theta \end{Bmatrix} Rd\theta dz \qquad (36)$$

and analogously for the other coefficients.

The flow from the two sides of the bearing is computed as:

$$Q = \sum_p -2 \int_{\theta_{1p}}^{\theta_{2p}} \frac{h_o^3}{12\mu} \left(\frac{\partial p_o}{\partial z}\right)_{z=\frac{1}{2}L} Rd\theta \qquad (37)$$

which does not include any flow in and out of the grooves.

The power loss is calculated from[1]:

$$P = \omega\Sigma_p[\mu R^3\omega \int_{\theta'_{1p}}^{\theta'_{2p}} \ell\frac{d\theta}{h_o} + \tfrac{1}{2}e_{op}(F_{xop}\sin\phi_{op} - F_{yop}\cos\phi_{op})] \quad (38)$$

where θ'_{1p} and θ'_{2p} give the groove positions for the pad, and ℓ equals the bearing length, L, except in any ruptured film zone where ℓ gives the width of the contracted film:

$$\ell = \ell(\theta) = \frac{1}{h}\int_B h dz \quad (39)$$

The indicated integration is performed either along the trailing end boundary curve or, when rupture occurs before the film forms, it is along the edge of the inlet groove.

The temperature rise through the film is determined from the energy equation[1]. With the simplifying assumptions that the flow is purely Couette flow (shear flow), that no heat is lost to the bearing or the journal, and that the viscosity is constant, the temperature increase becomes:

$$\Delta T = T_{out} - T_{in} = \frac{2}{c_v}\mu R^2\omega \int_{\theta_{1p}}^{\theta_{2p}} \frac{d\theta}{h^2} \quad (40)$$

where c_v is the specific heat per unit volume.

The equations are evaluated numerically and solved in finite difference form[1]. The finite difference grid with coordinates i and j has its j-axis along the θ-direction and the i-axis in the negative z-direction such that j=0 at $\theta=\theta_{1p}$, j=m at $\theta=\theta_{2p}$, i=0 at $z=\frac{1}{2}L$, and i=n at z=0. The finite difference increments are: $\Delta\theta=(\theta_{2p}-\theta_{1p})/m$ and $\Delta z=L/2n$. Thus, equation(27) is transformed into a finite difference equaion:

$$b_{j+1}p_{i,j+1} + b_{j-1}p_{i,j-1} + \alpha_j p_{i-1,j} + a_j p_{ij} + \alpha_j p_{i+1,j} = f_{ij} \quad (41)$$

where p_{ij} is the pressure at the point: $\theta_j=\theta_{1p}+j\Delta\theta$, $z_i=\frac{1}{2}L-i\Delta z$, f_{ij} is the right hand side of equation(27) evaluated at the same point, and the coefficients are:

$$b_{j-1} = \frac{h_{j-\frac{1}{2}}^3}{12\mu(R\Delta\theta)^2} \qquad b_{j+1} = \frac{h_{j+\frac{1}{2}}^3}{12\mu(R\Delta\theta)^2} \tag{42}$$

$$\alpha_j = \frac{h_j^3}{12\mu\Delta z^2} \qquad a_j = -(b_{j-1}+b_{j+1}+2\alpha_j)$$

Whereas h_j applies at $\theta=\theta_j$, $h_{j-\frac{1}{2}}$ is evaluated at $\theta=\theta_j-\frac{1}{2}\Delta\theta$, and $h_{j+\frac{1}{2}}$ at $\theta=\theta_j+\frac{1}{2}\Delta\theta$. At points neighbouring the rupture zone boundary the coefficients are modified to account for the local change in the difference increments $\Delta\theta$ and Δz[3].

Various iterative methods may be employed to solve equation(41). Because the equation, however, has to be solved five times with differing right hand sides the method of [2] offers many advantages. Here, equation(41) is written in matrix form as:

$$A_j\Phi_j+B_j\Phi_{j-1}+C_j\Phi_{j+1} = F_j \tag{43}$$

where Φ_j and F_j are column vectors whose i'th element is given by:

$$(\Phi_j)_i = p_{ij} \qquad (F_j)_i = f_{ij} \qquad \underline{1\leq i\leq n} \tag{44}$$

A_j is a tridiagonal matrix with the elements:

$$(A_j)_{ii} = a_j \qquad \underline{1\leq i\leq n}$$

$$(A_j)_{i,i+1} = \alpha_j \qquad \underline{1\leq i\leq n-1}$$

$$(A_j)_{i,i-1} = \begin{cases} \alpha_j & \underline{2\leq i\leq n-1} \\ 2\alpha_j & \underline{i=n} \end{cases} \tag{45}$$

which includes the boundary conditions at $z=\frac{1}{2}L$ and at $z=0$ (equations(28) and (29)).

B_j and C_j are diagonal matrices:

$$(B_j)_{ii} = b_{j-1} \qquad (C_j)_{ii} = b_{j+1} \qquad \underline{1\leq i\leq n} \tag{46}$$

The remaining elements of the three matrices are zero.

Equation(43) is solved by introducing a recurrence relationship:

$$\Phi_{j-1} = D_{j-1}\Phi_j + E_{j-1} \tag{47}$$

where D_j is a square matrix and E_j is a column vector. They are determined by substituting equation(47) into equation(43) to get:

$$D_j = -(A_j + B_j D_{j-1})^{-1} C_j$$

$$E_j = (A_j + B_j D_{j-1})^{-1} (F_j - B_j E_{j-1}) \tag{48}$$

For j=1, equation(48) is satisfied when $D_o=0$ and E_o equals the pressure at the θ_{1p}-boundary, Φ_o, usually zero. Then equation(48) can be used to calculate D_j and E_j, starting with j=1 and going to j=m-1. Thereafter the pressure distribution, Φ_j, is found by backsubstitution from equation(47), letting j go from m to 2(ϕ_m is zero, namely equal to the pressure at θ_{2p}).

The savings in computation time is obtained by storing the inverted matrices: $(A_j+B_jD_{j-1})^{-1}$during solving the first of equation(27), after which the remaining four equations for the pressure pertubations are evaluated by simple matrix multiplication.

When calculating the static pressure, p_o, by means of the backsubstitution of equation(47), any encountered negative pressure value is set equal to zero before proceeding to the next j-value (this does not apply to the perturbed pressures). The resulting pressure profile will have the required zero gradient at the boundary to the ruptured film zone, but to locate the boundary curve properly a third order polynominal is fitted through the three pressure values closest to the boundary for each i-grid line. In this way, the θ-coordinates for the boundary curve, namely θ_{2p}, are determined after which the finite difference increments are adjusted accordingly, and a new calculation of the pressure distribution is performed. The procedure is repeated until the difference between two successive iterations is suitable small, say of the order of 10^{-5}in pressure values, requiring typically 5 to 10 iterations.

With the rupture boundary curve established, the pressure distributions may be integrated numerically to give the static load and the dynamic coefficients in accordance with equations(35) and (36).

Similarly, the flow, the power loss and the temperature rise are computed from equations(37), (38) and (40).

The calculations are based on some selected value of the journal center eccentricity, e, and an estimated value of the associated attitude angle, ϕ(the corresponding pad eccentricities, e_p, and attitude angles, ϕ_p, are obtained from equations(19) and (20)). If the horizontal component, F_{yo}, of the bearing reaction force is not zero the calculations are repeated with a new attitude angle value until the error becomes less than 0.001 degrees.

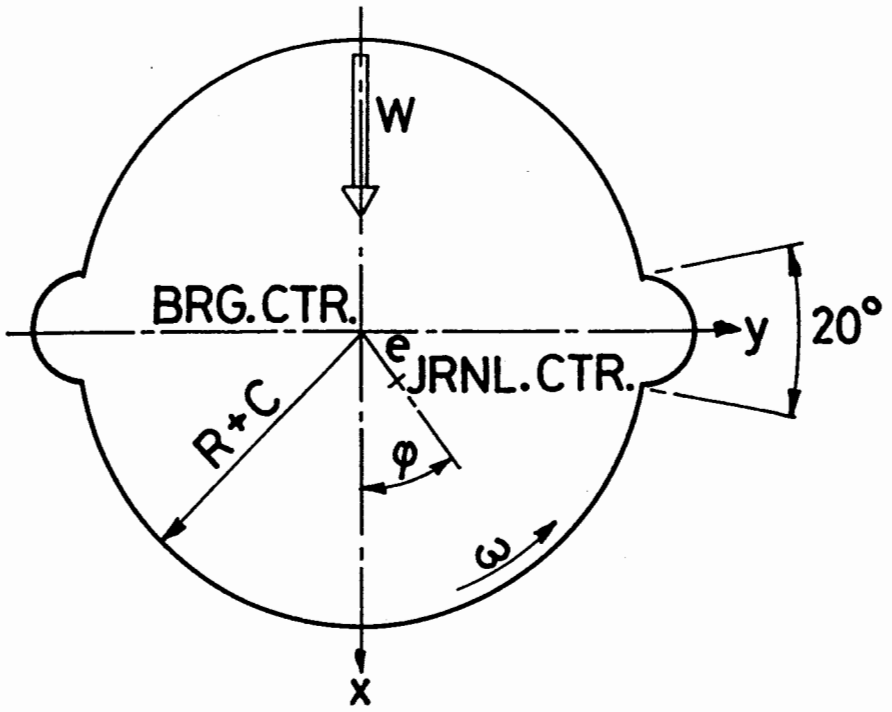

TWO AXIAL-GROOVE

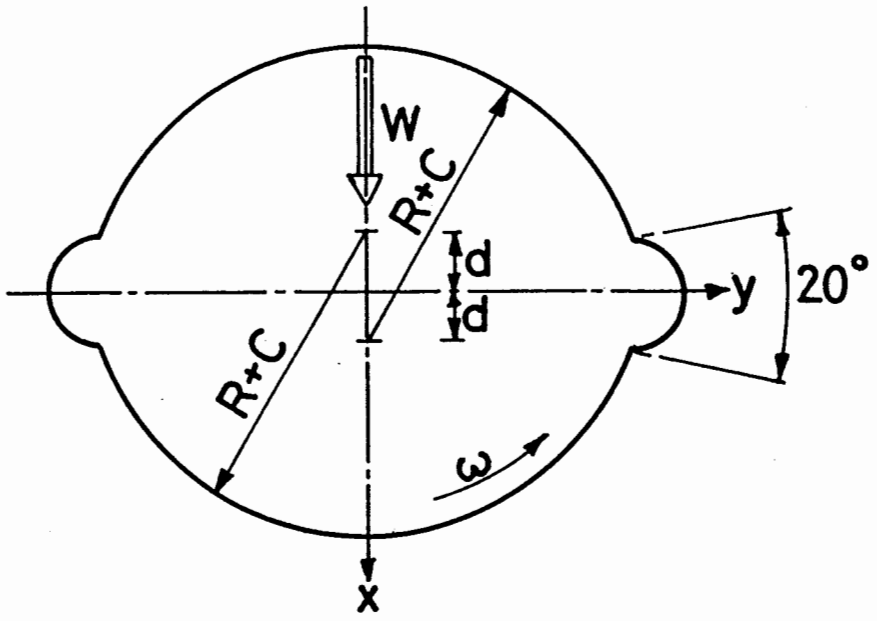

ELLIPTICAL

Fig. 1 Bearing types

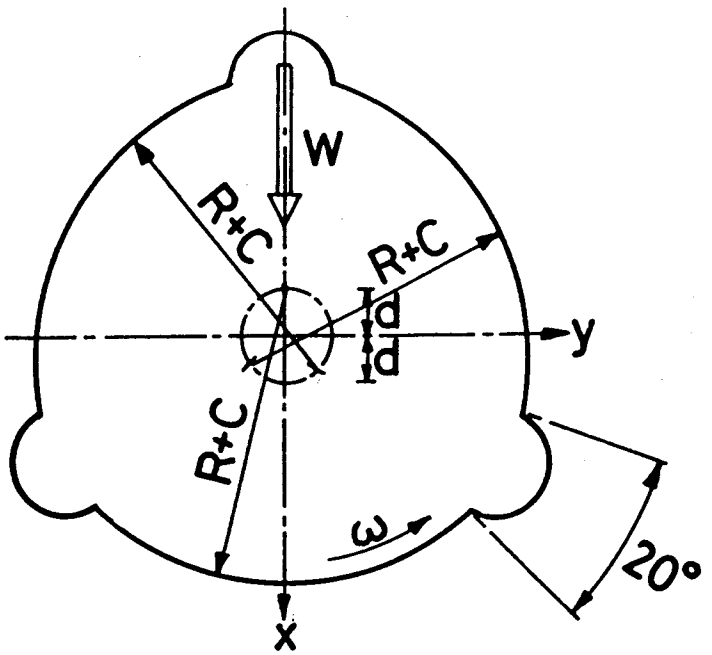

THREE-LOBE

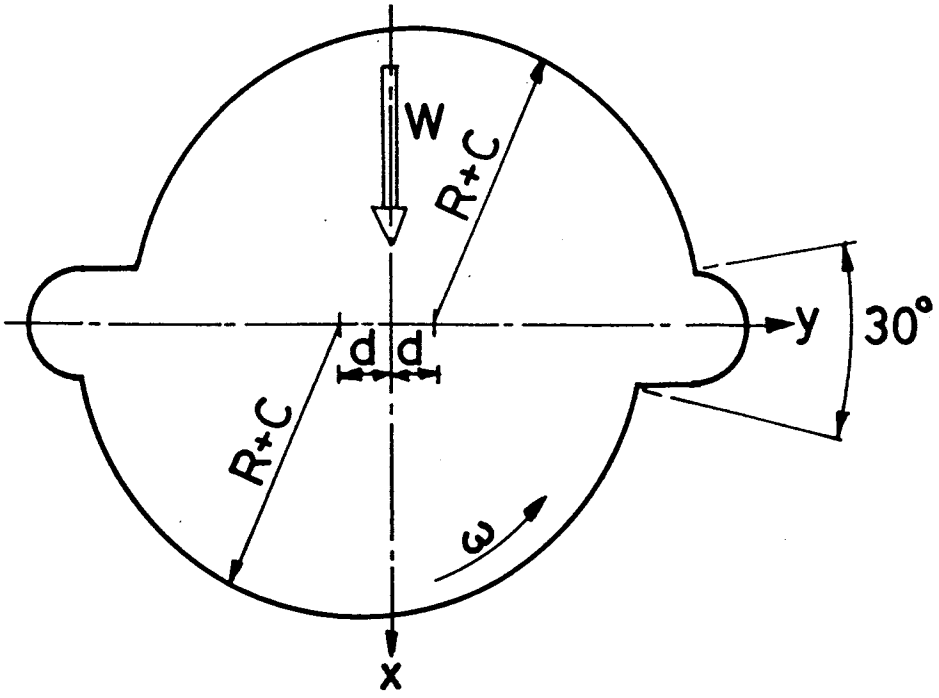

OFFSET CYLINDRICAL

(continued)

Fig. 1 Bearing types

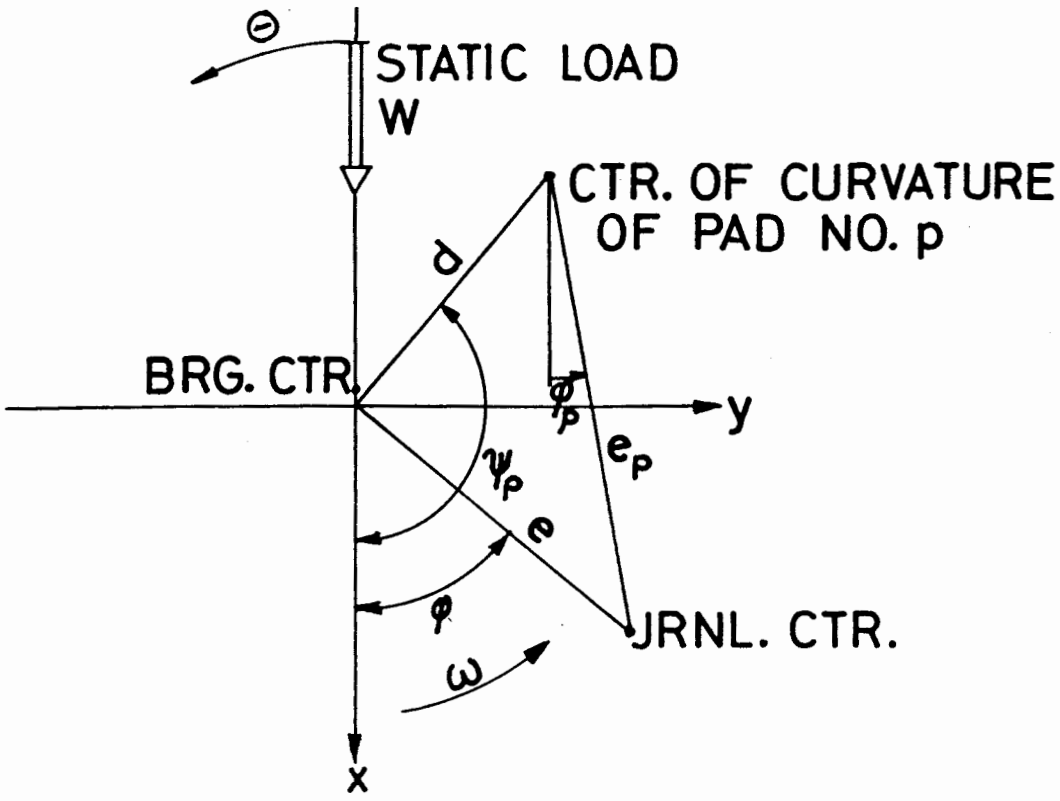

Fig. 2 Journal center coordinates

Table 1a Two-axial-groove bearing, L/D = 0.5

S	ε	ϕ	$\bar{Q}$	$\bar{P}$	$\bar{T}$	$\bar{K}_{xx}$	$\bar{K}_{xy}$	$\bar{K}_{yx}$	$\bar{K}_{yy}$	$\bar{B}_{xx}$	$\bar{B}_{xy}=\bar{B}_{yx}$	$\bar{B}_{yy}$
6.430	0.071	81.89	0.121	0.860	5.7	1.55	14.41	-6.60	1.88	28.75	1.89	13.31
3.937	0.114	77.32	0.192	0.846	5.9	1.57	9.27	-4.20	1.89	18.44	1.93	8.58
2.634	0.165	72.36	0.271	0.833	6.2	1.61	6.74	-3.01	1.91	13.36	2.00	6.28
2.030	0.207	68.75	0.332	0.835	6.6	1.65	5.67	-2.50	1.93	11.18	2.07	5.33
1.656	0.244	65.85	0.383	0.835	7.0	1.69	5.06	-2.20	1.95	9.93	2.15	4.80
0.917	0.372	57.45	0.540	0.850	8.5	2.12	4.01	-1.30	1.85	7.70	2.06	3.23
0.580	0.477	51.01	0.651	0.900	10.5	2.67	3.70	-0.78	1.75	6.96	1.94	2.40
0.378	0.570	45.43	0.737	0.977	13.4	3.33	3.64	-0.43	1.68	6.76	1.87	1.89
0.244	0.655	40.25	0.804	1.096	17.9	4.21	3.74	-0.13	1.64	6.87	1.82	1.54
0.194	0.695	37.72	0.833	1.156	21.3	4.78	3.84	0.01	1.62	7.03	1.80	1.40
0.151	0.734	35.20	0.858	1.240	25.8	5.48	3.98	0.15	1.61	7.26	1.79	1.27
0.133	0.753	33.93	0.870	1.289	28.7	5.89	4.07	0.22	1.60	7.41	1.79	1.20
0.126	0.761	33.42	0.875	1.310	30.0	6.07	4.11	0.25	1.60	7.48	1.79	1.18
0.116	0.772	32.65	0.881	1.343	32.2	6.36	4.17	0.30	1.60	7.59	1.79	1.15
0.086	0.809	30.04	0.902	1.473	41.4	7.51	4.42	0.47	1.59	8.03	1.79	1.03
0.042	0.879	24.41	0.936	1.881	80.9	11.45	5.23	0.92	1.60	9.48	1.80	0.82

Table 1b Two-axial-groove bearing, L/D = 1

S	ε	ϕ	$\bar{Q}$	$\bar{P}$	$\bar{T}$	$\bar{K}_{xx}$	$\bar{K}_{xy}$	$\bar{K}_{yx}$	$\bar{K}_{yy}$	$\bar{B}_{xx}$	$\bar{B}_{xy}=\bar{B}_{yx}$	$\bar{B}_{yy}$
1.470	0.103	75.99	0.135	0.850	5.9	1.53	10.14	-3.01	1.50	20.34	1.53	6.15
0.991	0.150	70.58	0.189	0.844	6.2	1.56	7.29	-2.16	1.52	14.66	1.58	4.49
0.635	0.224	63.54	0.264	0.843	6.9	1.62	5.33	-1.57	1.56	10.80	1.70	3.41
0.358	0.352	55.41	0.369	0.853	8.7	1.95	3.94	-0.97	1.48	8.02	1.63	2.37
0.235	0.460	49.27	0.436	0.914	11.1	2.19	3.57	-0.80	1.55	7.36	1.89	2.19
0.159	0.559	44.33	0.484	1.005	14.2	2.73	3.36	-0.48	1.48	6.94	1.78	1.74
0.108	0.650	39.72	0.516	1.136	19.2	3.45	3.34	-0.23	1.44	6.89	1.72	1.43
0.071	0.734	35.16	0.534	1.323	27.9	4.49	3.50	0.03	1.44	7.15	1.70	1.20
0.056	0.773	32.82	0.540	1.449	34.9	5.23	3.65	0.18	1.45	7.42	1.71	1.10
0.050	0.793	31.62	0.541	1.524	39.6	5.69	3.75	0.26	1.45	7.60	1.71	1.06
0.044	0.811	30.39	0.543	1.608	45.3	6.22	3.88	0.35	1.46	7.81	1.72	1.01
0.024	0.883	25.02	0.543	2.104	89.6	9.77	4.69	0.83	1.53	9.17	1.78	0.83

Table 2a Elliptical bearing, preload: $\delta = 0.5$, L/D = 0.5

S	ϵ	ϕ	$\bar{Q}$	$\bar{P}$	$\bar{T}$	$\bar{K}_{xx}$	$\bar{K}_{xy}$	$\bar{K}_{yx}$	$\bar{K}_{yy}$	$\bar{B}_{xx}$	$\bar{B}_{xy}=\bar{B}_{yx}$	$\bar{B}_{yy}$
7.079	0.024	88.79	0.512	1.313	9.8	91.58	40.32	-57.12	1.29	159.20	-63.29	45.50
2.723	0.061	88.58	0.518	1.315	10.0	35.54	15.77	-22.03	0.74	61.63	-23.96	17.80
1.889	0.086	88.33	0.525	1.318	10.3	24.93	11.18	-15.33	0.71	43.14	-16.31	12.59
1.229	0.127	87.75	0.541	1.325	10.8	16.68	7.66	-10.03	0.78	28.65	-10.11	8.57
0.976	0.155	87.22	0.555	1.332	11.2	13.59	6.39	-7.99	0.84	23.20	-7.66	7.08
0.832	0.176	86.75	0.567	1.338	11.6	11.88	5.69	-6.82	0.90	20.14	-6.23	6.23
0.494	0.254	84.36	0.624	1.371	13.5	8.11	4.28	-3.99	1.09	13.26	-2.76	4.27
0.318	0.323	81.08	0.684	1.421	16.4	6.52	3.82	-2.34	1.23	10.03	-0.81	3.15
0.236	0.364	78.09	0.723	1.468	19.4	6.07	3.76	-1.49	1.31	8.80	0.11	2.54
0.187	0.391	75.18	0.747	1.515	22.6	6.03	3.82	-0.92	1.37	8.23	0.66	2.13
0.153	0.410	72.26	0.762	1.562	26.1	6.21	3.92	-0.52	1.41	7.98	1.02	1.82
0.127	0.424	69.31	0.770	1.612	30.1	6.53	4.04	-0.21	1.45	7.91	1.26	1.58
0.090	0.444	63.24	0.772	1.727	40.1	7.55	4.33	0.23	1.50	8.11	1.54	1.23

Table 2b Elliptical bearing, preload: $\delta = 0.5$, L/D = 1

	S	ε	♦	$\bar{Q}$	$\bar{P}$	$\bar{T}$	$\bar{K}_{xx}$	$\bar{K}_{xy}$	$\bar{K}_{yx}$	$\bar{K}_{yy}$	$\bar{B}_{xx}$	$\bar{B}_{xy}=\bar{B}_{yx}$	$\bar{B}_{yy}$
1	1.442	0.050	93.81	0.309	1.338	10.8	38.58	22.65	-22.14	-1.29	79.05	-28.14	18.60
2	0.698	0.100	93.12	0.320	1.345	11.2	18.93	11.25	-10.79	-0.24	38.73	-12.97	9.40
3	0.442	0.150	91.97	0.338	1.357	11.9	12.28	7.45	-6.87	0.26	25.00	-7.50	6.36
4	0.308	0.200	90.37	0.361	1.376	12.8	8.93	5.58	-4.79	0.58	17.99	-4.50	4.82
5	0.282	0.213	89.87	0.368	1.382	13.1	8.30	5.24	-4.38	0.66	16.66	-3.91	4.53
6	0.271	0.220	89.61	0.372	1.385	13.2	8.03	5.09	-4.20	0.69	16.08	-3.64	4.40
7	0.261	0.226	89.37	0.375	1.388	13.4	7.79	4.96	-4.03	0.72	15.57	-3.41	4.28
8	0.240	0.239	88.80	0.383	1.396	13.7	7.31	4.70	-3.70	0.77	14.54	-2.93	4.04
9	0.224	0.250	88.28	0.389	1.403	14.1	6.95	4.51	-3.43	0.82	13.74	-2.55	3.86
10	0.211	0.260	87.79	0.395	1.409	14.4	6.65	4.36	-3.21	0.86	13.09	-2.23	3.70
11	0.161	0.304	85.29	0.423	1.445	16.2	5.63	3.84	-2.32	1.01	10.75	-1.02	3.07
12	0.120	0.350	81.80	0.452	1.500	19.1	4.99	3.54	-1.52	1.14	9.04	-0.01	2.49
13	0.097	0.381	78.65	0.470	1.554	22.1	4.82	3.46	-1.01	1.21	8.26	0.56	2.10
14	0.081	0.403	75.63	0.479	1.607	25.4	4.87	3.47	-0.65	1.26	7.87	0.92	1.82
15	0.069	0.419	72.65	0.484	1.664	29.1	5.06	3.52	-0.38	1.31	7.71	1.17	1.60
16	0.060	0.432	69.69	0.485	1.724	33.4	5.36	3.60	-0.16	1.34	7.67	1.34	1.42
17	0.045	0.451	63.70	0.478	1.867	44.3	6.25	3.83	0.19	1.40	7.88	1.56	1.16

Table 3a Three-lobe bearing, preload: $\delta = 0.5$, L/D = 0.5

S	ε	ϕ	$\bar{Q}$	$\bar{P}$	$\bar{T}$	$\bar{K}_{xx}$	$\bar{K}_{xy}$	$\bar{K}_{yx}$	$\bar{K}_{yy}$	$\bar{B}_{xx}$	$\bar{B}_{xy}=\bar{B}_{yx}$	$\bar{B}_{yy}$
6.574	0.018	55.45	0.250	1.420	8.2	34.58	45.43	-46.78	31.32	97.87	-1.46	93.55
3.682	0.031	56.03	0.251	1.421	8.5	20.35	25.35	-26.57	17.08	56.10	-1.35	51.73
2.523	0.045	56.57	0.252	1.423	8.9	14.75	17.41	-18.48	11.48	39.52	-1.22	35.06
1.621	0.070	57.35	0.255	1.429	9.5	10.53	11.38	-12.20	7.25	26.81	-1.01	22.25
1.169	0.094	57.95	0.259	1.437	10.2	8.56	8.49	-9.06	5.26	20.62	-0.79	15.96
0.717	0.144	58.62	0.271	1.461	11.8	6.85	5.85	-5.92	3.49	14.74	-0.37	9.93
0.491	0.192	58.63	0.285	1.497	13.8	6.27	4.75	-4.34	2.77	12.07	0.02	7.12
0.356	0.237	58.14	0.300	1.543	16.2	6.15	4.26	-3.35	2.41	10.67	0.36	5.51
0.267	0.278	57.30	0.315	1.599	19.1	6.29	4.05	-2.63	2.19	9.87	0.66	4.46
0.203	0.314	56.18	0.331	1.665	22.8	6.62	4.00	-2.05	2.04	9.43	0.91	3.68
0.156	0.347	54.85	0.345	1.742	27.6	7.11	4.05	-1.55	1.90	9.23	1.12	3.06
0.141	0.360	54.26	0.352	1.776	29.8	7.35	4.10	-1.36	1.85	9.20	1.20	2.84
0.121	0.377	53.31	0.361	1.830	33.6	7.77	4.19	-1.09	1.78	9.20	1.30	2.54
0.093	0.402	51.55	0.379	1.931	41.6	8.63	4.39	-0.67	1.67	9.30	1.44	2.10
0.055	0.441	47.10	0.419	2.182	66.1	11.07	4.94	0.14	1.49	9.91	1.61	1.29

Table 3b Three-lobe bearing, preload: $\delta = 0.5$, L/D = 1

S	ε	ϕ	$\bar{Q}$	$\bar{P}$	$\bar{T}$	$\bar{K}_{xx}$	$\bar{K}_{xy}$	$\bar{K}_{yx}$	$\bar{K}_{yy}$	$\bar{B}_{xx}$	$\bar{B}_{xy}=\bar{B}_{yx}$	$\bar{B}_{yy}$
3.256	0.020	59.21	0.132	1.424	8.8	28.31	43.30	-43.40	25.25	94.58	-1.11	88.33
1.818	0.035	59.68	0.133	1.426	9.2	16.74	24.39	-24.34	13.70	54.59	-0.98	48.27
1.243	0.050	60.09	0.134	1.429	9.6	12.21	16.93	-16.72	9.18	38.75	-0.84	32.37
0.796	0.076	60.62	0.136	1.436	10.4	8.82	11.26	-10.82	5.80	26.62	-0.61	20.18
0.574	0.103	60.95	0.139	1.447	11.2	7.24	8.55	-7.90	4.24	20.73	-0.37	14.27
0.353	0.155	61.00	0.147	1.478	13.0	5.91	6.07	-5.02	2.89	15.15	0.06	8.70
0.245	0.203	60.44	0.156	1.521	15.2	5.48	5.01	-3.60	2.36	12.59	0.43	6.16
0.181	0.246	59.46	0.165	1.574	17.8	5.41	4.49	-2.74	2.09	11.20	0.73	4.73
0.138	0.285	58.22	0.173	1.637	21.0	5.54	4.22	-2.12	1.92	10.39	0.98	3.81
0.108	0.320	56.80	0.181	1.710	24.9	5.83	4.10	-1.65	1.80	9.91	1.18	3.16
0.085	0.351	55.23	0.189	1.794	29.9	6.25	4.08	-1.26	1.71	9.64	1.35	2.67
0.068	0.379	53.54	0.197	1.891	36.2	6.82	4.13	-0.92	1.62	9.54	1.48	2.29
0.062	0.389	52.82	0.201	1.934	39.2	7.09	4.17	-0.79	1.59	9.54	1.52	2.16
0.054	0.403	51.68	0.208	2.014	44.4	7.56	4.25	-0.57	1.54	9.57	1.57	1.92
0.034	0.441	47.19	0.232	2.290	69.8	9.70	4.65	0.11	1.42	10.03	1.67	1.23

Table 4a Offset cylindrical bearing, preload: $\delta = 0.5$, $L/D = 0.5$

S	ε	ϕ	$\bar{Q}$	$\bar{P}$	$\bar{T}$	$\bar{K}_{xx}$	$\bar{K}_{xy}$	$\bar{K}_{yx}$	$\bar{K}_{yy}$	$\bar{B}_{xx}$	$\bar{B}_{xy}=\bar{B}_{yx}$	$\bar{B}_{yy}$
8.519	0.025	-4.87	1.664	0.971	7.7	47.06	82.04	5.48	64.74	97.59	45.00	59.71
4.240	0.050	-4.82	1.664	0.972	8.0	23.60	41.06	2.64	32.32	49.04	22.62	29.94
2.805	0.075	-4.72	1.664	0.975	8.4	15.81	27.42	1.65	21.49	32.97	15.22	20.06
2.081	0.100	-4.59	1.664	0.978	8.8	11.93	20.61	1.12	16.05	25.01	11.56	15.15
1.339	0.150	-4.14	1.660	0.988	9.7	8.08	13.79	0.54	10.56	17.15	7.98	10.25
0.953	0.200	-3.47	1.649	1.002	10.8	6.18	10.39	0.20	7.78	13.34	6.31	7.83
0.717	0.250	-2.76	1.641	1.023	12.1	5.14	8.45	-0.05	6.15	11.29	5.43	6.51
0.555	0.300	-2.02	1.637	1.036	13.7	4.63	7.20	-0.09	5.00	10.00	4.76	5.38
0.493	0.325	-1.78	1.637	1.052	14.3	4.56	6.72	0.01	4.53	9.49	4.38	4.74
0.353	0.400	-1.70	1.645	1.108	16.5	4.63	5.78	0.22	3.53	8.51	3.56	3.40
0.284	0.450	-2.00	1.656	1.154	18.4	4.85	5.40	0.33	3.08	8.17	3.18	2.79
0.228	0.500	-2.51	1.671	1.210	21.0	5.18	5.15	0.42	2.74	7.99	2.88	2.34
0.182	0.551	-3.19	1.690	1.276	24.4	5.65	5.01	0.51	2.48	7.95	2.65	1.98
0.162	0.576	-3.58	1.700	1.314	26.5	5.93	4.97	0.55	2.37	7.97	2.55	1.82
0.143	0.601	-4.02	1.711	1.357	28.9	6.26	4.95	0.60	2.27	8.02	2.46	1.69
0.126	0.627	-4.49	1.723	1.404	31.9	6.64	4.95	0.65	2.19	8.10	2.38	1.56

Table 4b Offset cylindrical bearing, preload: $\delta = 0.5$, $L/D = 1$

S	ε	ϕ	$\bar{Q}$	$\bar{P}$	$\bar{T}$	$\bar{K}_{xx}$	$\bar{K}_{xy}$	$\bar{K}_{yx}$	$\bar{K}_{yy}$	$\bar{B}_{xx}$	$\bar{B}_{xy}=\bar{B}_{yx}$	$\bar{B}_{yy}$
3.780	0.025	-8.21	1.271	1.030	7.7	52.13	83.73	8.14	56.69	113.96	42.08	47.10
1.883	0.051	-8.16	1.271	1.031	8.0	26.11	41.89	3.99	28.31	57.20	21.13	23.61
1.247	0.076	-8.08	1.271	1.034	8.3	17.45	27.95	2.57	18.83	38.38	14.19	15.81
0.927	0.101	-7.96	1.271	1.037	8.7	13.13	20.99	1.83	14.08	29.04	10.75	11.93
0.596	0.151	-7.46	1.266	1.047	9.5	8.74	13.89	1.05	9.22	19.61	7.33	8.00
0.418	0.201	-6.58	1.244	1.061	10.6	6.44	10.17	0.62	6.68	14.73	5.64	5.96
0.316	0.251	-5.85	1.224	1.081	11.8	5.22	8.13	0.33	5.26	12.18	4.78	4.90
0.248	0.301	-5.10	1.206	1.105	13.3	4.49	6.87	0.11	4.35	10.71	4.30	4.28
0.198	0.351	-4.29	1.191	1.133	15.3	4.08	6.02	-0.04	3.70	9.80	3.99	3.83
0.160	0.401	-3.59	1.179	1.168	17.4	4.00	5.40	0.01	3.17	9.07	3.57	3.22
0.130	0.451	-3.27	1.171	1.223	19.6	4.13	4.96	0.12	2.76	8.55	3.15	2.65
0.107	0.501	-3.28	1.166	1.289	22.4	4.37	4.68	0.22	2.46	8.23	2.84	2.22
0.087	0.551	-3.54	1.165	1.369	26.1	4.74	4.50	0.31	2.23	8.08	2.60	1.89
0.078	0.576	-3.76	1.166	1.415	28.5	4.98	4.45	0.36	2.14	8.06	2.50	1.75
0.070	0.601	-4.03	1.167	1.466	31.2	5.25	4.42	0.41	2.06	8.07	2.42	1.63